Structural design and verification of an innovative whole adaptive variable camber wing

Anmin Zhao[a,b], Hui Zou[a], Haichuan Jin[a], Dongsheng Wen[a]

[a]National key Laboratory of Human Machine and Environment Engineering, Beihang University, Beijing, 100191, China

[b]National key laboratory of Computational Fluid Dynamics, Beihang University, Beijing, 100191, China

Abstract: A whole adaptive variable camber wing (AVCW) equipped with an innovative double rib sheet (DRS) structure is experimentally and numerically studied in this work. The new design uses surface contact of DRS for force transmission of changeable camber wing instead of the traditional rigid hinge joint contact. The AVCW design allows the change of airfoil camber in a real-time process under different flight states and flight environment, which is of great interest tof Unmanned Aerial Vehicle (UAV) applications.. Numerical results show that the used of the varying camber airfoil has better stalled characteristic and aerodynamic performance comparing with the Clark Y and AH-79-100C airfoil. . The flight-test experiments indicate that the total AVCW carrying the autonomous development adaptive control system (ACS) can further enhance UAV flight efficiency by 29.4% relative to Talon UAV. It suggests that using AVCW structural can increase the load capacity and improve flight efficiency, without increasing the overall structural weight, which is promising for future engineering application to the UAV field.

Keywords:

Double Rib Sheet (DRS), whole Adaptive Variable Camber Wing (AVCW), adaptive control system (ACS), flight efficiency;

1. Introduction

Modern unmanned aerial vehicles (UAVs) are mainly designed to improve flight efficiency in multi-environment and multi-missions flight, in which an adaptive variable camber wing (AVCW) is the most essential [1-4]. Traditional AVCW design schemes are based on mechanical hinge transmission to accomplish the change of the wing camber. Such scheme, however, suffers many limitations as the hinge parts are heavy and the contact surfaces are point-contact, which results in not only a low operation efficient but also a stress concentration prone to structure failure.

Many attempts have been performed to overcome such problems. . In the 1980s', mission-adaptive wing technology research was launched by the National Advisory Committee for Aeronautics (NASA) and the Boeing Company. It was suggested that the traditional control surface could be replaced by a flexible composite material skin operated by a digital flight control system, leading to increased lift-drag ratio and delayed flow separation on the wing surface. However, the complexity and heavy weight of mechanistic drivers obstruct its practical application [5-7]. In recent years, many studies on variable camber morphing wing have been conducted regarding the aerodynamic and structure performance of conventional leading-edge and trailing-edge of wings, but the whole changeable camber wing has not been considered. Stanford et al. investigated the static and dynamic aeroelastic tailoring with variable camber control, and showed that the wing structural weight could be reduced by adopting variable camber continuous trailing-edge flap system with improved aeroelastic behavior of the wing [8] . It has been reported that a variable camber fowler flap aerodynamic performance with a double-sliding track can be used for general aviation aircraft. The maximum lift coefficient was increased by 6.6% and ratio of lift-to-drag was decreased by 7.58% relative to the reference conventional fowler flap model [9]. Moreover, some inconstant camber wing structure investigations have been effectively carried out by [10-13]. It was indicated that the variable camber morphing wing, which was composed of corrugated structures, was feasible by considering both numerical simulation and wind tunnel experimenta results. Furthermore, the deformation of morphing skin is determined by the bending stiffness of the material, which could be studied by the flexible shin stiffness requirement of variable wings.

Using new materials as an actuator of variable camber wings has received strong interest. The surface deformation of the UAVs altered by a piezoelectric ceramic structure was designed (FlexSys Inc, U.S), resulting in reduced weight and increased cruise time of the UAVs [14]. Kota et al. investigated a flexible skin covering on the trailing edge of the wing and realized the deformation of the wing by smoothly bending the flexible trailing edge [15]. A variable camber wing was demonstrated by Beihang University (Li et al.,2009), which used the shape memory alloy (SMA) as the actuators to change wing camber. It was indicated that the average lift of the wing was improved by 20% in the wind tunnel experimental [16]. A variable trailing camber wing model was designed and made of SMA material, good actuation performance even in condition of external loads was demonstrated both numerically and experimentally [17]. A novel 0-Poisson's ratio cosine honeycomb support structure of flexible skin was proposed by Liu et al, which could reduce power consumption and driving force [18]. Li and Ang conducted an innovative adaptive variable camber compliant wing based on a new artificial muscle in [10]. The results showed that this method could design airfoils for this morphing wing in a quick and effective way. Some similar works also have been implemented by [19, 20]. Nevertheless, expensive smart materials and device instability restrict its wide engineering application.

It is clearly from the review that that although extensive research has been performed for the aerodynamic, structure and material of the leading-edge or trailing-edge variable camber wings, the investigation of a whole AVCW has not yet been reported. This work aims to develop an innovative DRS structure that can realize the change of the whole camber of wing. 2D and 3D numerical simulations are conducted to investigate the influence of the camber change on the aerodynamic characteristics of the changeable airfoil and wing at different angles of attack. A prototype model of the complete varying camber wing is manufactured, and tested on ground and flight experiments. The flight-test results show that employing whole AVCW technology improves flight efficiency by ~ 29%.

2. Structural model of the whole variable camber wing

In order to define the deflection angle of the variable camber airfoil, a symmetrical airfoil, NACA 0012, is selected with the chord length L of 330mm [Fig. 1(a)]. A four-section airfoil is designed to obtain the whole camber change of airfoil in the proportion of 1:2:2:1. Illustrated in Figure 1(a), the four-typical state of airfoil is chosen to investigate the change of airfoil camber. The airfoil (NACA 0012) is modified to realize a smooth transition of airfoil to improve aerodynamics performance. To verify the flow advantages of variable camber airfoil profile of 2D, Clark Y airfoil and AH-79-100C airfoil are selected for comparison, as shown in Figure 1-b.

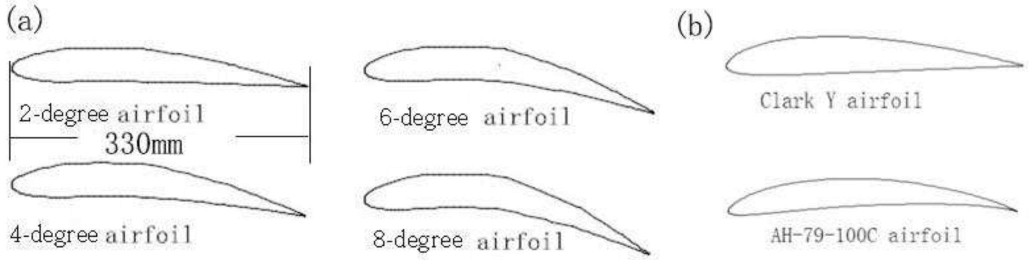

Figure 1. Schematic diagram of 2D airfoil: (a) 4-variable camber airfoil profiles, and (b) 2-convention low-speed contrast airfoils.

A double rib sheet (DRS) structure is invented, as shown in Figure 2, to realize the overall wing camber change. The structural has one side of a semicircular groove, and the other side of a circular ear, both of which are in closely contact. Via this way, the geometry configuration of the complete wing rib is connected by four double rib sheets. It is clear that such mechanical structure design will not increase the weight of the entire wing structure. In addition, the load transfer between the sections of the wing rib structures is transformed into surface contact from the traditional point contact, which could not only avoids the problem of stress concentration, but also allows the structure to bear greater load.

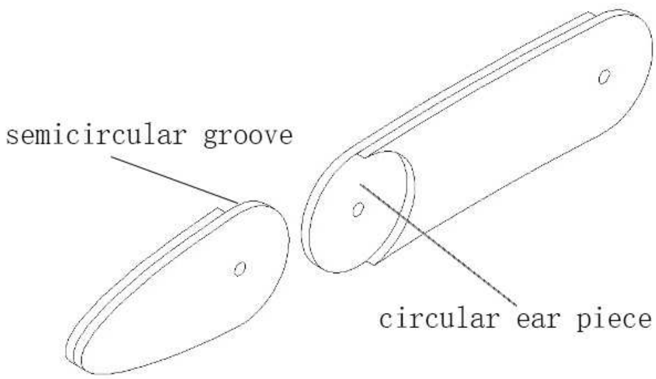

Figure 2. Double rib sheet structural model.

A schematic diagram of an innovation entire wing structure is presented in Figure3, with a total surface area of $0.5m^2$. The model is composed of wing rib, skin and wing spar, which is similar to the wing structure of general aviation aircraft, without the increase of additional weight except for the actuator. The wing rib model is composed of four separate wing structural sections, which include the wing leading edge section, wing trailing edge section, wing mid-section and the wing mid-aft section, respectively. The overall wing camber change is obtained by the relative rotation between the wing rib structure sections. Compared with traditional control mode, the variable camber wing can change the complete wing camber when the state and conditions of flying are varied. The test experiment of the whole changeable camber wing on the ground is shown in the supplementary material. It is known that conventional aircraft is designed to reach optimal performance characteristics only for a single mission. However, changes in the flight states and flight environment of UAV are inevitable, and the traditional fixed wing structure could not achieve a multi-missions optimal flight. . The design of AVCW shall address this issue by allowing real-time change of wing position by the active control system (ACS). In this way, the airfoil of the wing is always adjusted to the optimum state based on different flight states and flight environment. It is expected that comparing to the variable leading-edge camber wing or variable trailing-edge camber wing structure, employing the whole AVCW technology could improve further UAV aerodynamic characteristics and flight efficiencies, as shown by both numerical modelling and flight experiments below.

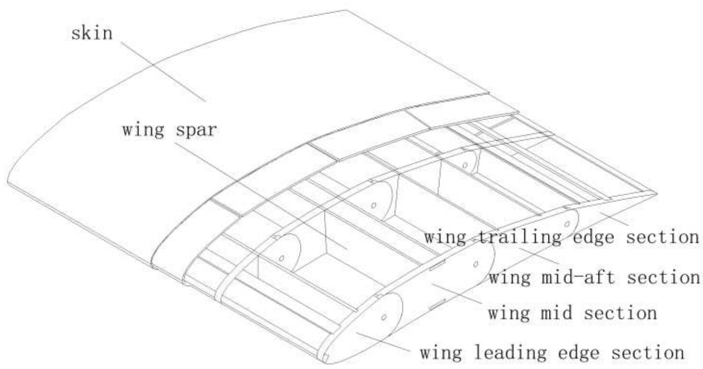

Figure 3. Variable camber wing structure model

3. Numerical simulation

3.1 D grid generation and boundary conditions of AVCW

A C-type structured grid is adopted in the ICEM CFD 15.0 [21] to discretize the flow field around airfoil two-dimensional model, as illustrated in Figure 4. The computational domain is selected to be big enough to avoid the influence of far-field boundary conditions on the flow characteristic of the model. The mesh extends to 15L from airfoil surface to the far-field boundary, i.e., the boundary length is 15L from upstream, downstream, the upper and lower boundaries respectively. Figure 4(a) shows the structured grid for the integral calculation domain, which is divided into two parts: 1(airfoil) and 2(far-field) for the inner and outer mesh, respectively. Figure 1(b) and 1(c) show an enlarged view of the airfoil profile and the quality of the grid is 0.76~0.866.

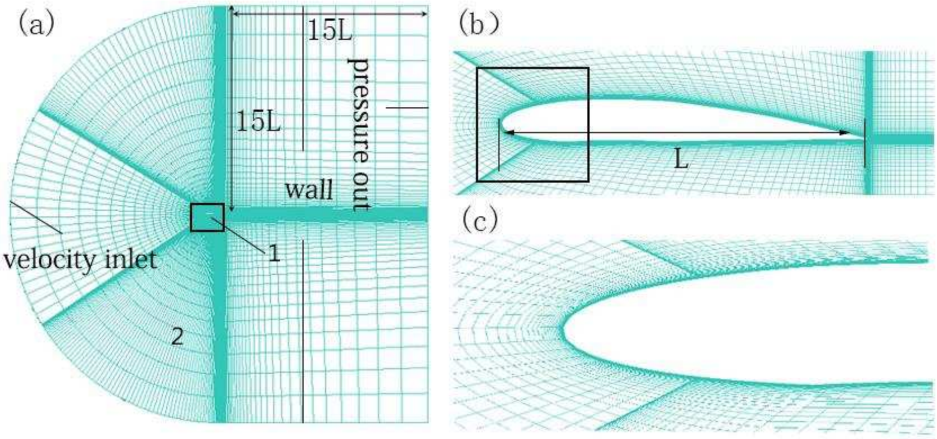

Figure 4. Schematic of the computation mesh and boundary conditions

The far-field boundary conditions are set as follows: the inlet boundary is the velocity inlet; the upper and lower boundary is the no-slip wall; and the out boundary is defined as pressure out, shown in Figure 4-a. The Reynolds number is given by

$$\mathrm{Re}=\frac{\rho L U_\infty}{\mu} \tag{1}$$

Where ρ , μ , U_∞ and L are air density 1.225 kg/m^3, air kinematic viscosity coefficient 1.7894×10^{-5} kg/(m gs), the free-velocity 18 m/s, and the chord length of airfoil 0.33m, respectively.

Based on the equation (1) and above constant, the Reynolds number is calculated as 406508. The drag and lift are parallel and perpendicular to the far-field free stream. The corresponding lift and drag coefficient can be given as

$$C_l=\frac{F_y}{0.5\rho U_\infty^2 S} \tag{2}$$

$$C_d=\frac{F_x}{0.5\rho U_\infty^2 S} \tag{3}$$

Where C_l is the lift coefficient, C_d is the drag coefficient, S is the area of the wing, F_x

and F_y are the drag and lift, respectively.

In order to ensure grid independence, four types of mesh with different grid density are employed to investigate lift and drag coefficients for a 2-degree airfoil shown in Figure 1 with the angles of attack of 6 ° and 10 ° respectively The simulation results in Table 1 show that the differences of drag and lift coefficients are within 4% between types 2 and 3. With further increase of grid cell density, the difference can be reduced to less than 3%. However for the consideration of both simulation accuracy and simulation time constrains, the grid density of type 2 is chosen in this work.

Table 1. Mesh independence study for variable camber airfoil at Re=406508 and angle of attack of 6 ° and 10 °

Type	Number of cells	Angle of attack 6 °		Angle of attack 10 °	
		C_L	C_d	C_L	C_d
1	15000	1.1152	0.78951	1.3125	0.4352
2	39500	1.1387	0.08078	1.3413	0.1447
3	88000	1.1806	0.08352	1.3822	0.1421
4	250000	1.1625	0.08452	1.3652	0.1435

The normal velocity of boundary layer is very substantial in the adjacent airfoil region, and the boundary grid Y spacing value set is critical to calculate the flow field of the near wall region. In this study, NACA Y+ wall distance estimation online is adopted, and the height of the first layer grid is calculated to 0.000128m. The universal computational fluid dynamics solver employed is the Spalart-Allmaras model (SA) [22]. In order to obtain an analogy wind tunnel tests condition, a no-slip boundary condition of the airfoil surface is applied.

3.2 3D grid generation and boundary conditions of AVCW

The unstructured grid is adopted in the ICEM CFD 15.0 [21] to discretize the flow field around the three-dimensional model, as is shown in Figure 5, with a size of the computational domain of 20L×10L×10L in the X, Y and Z direction, respectively. According to the demand of meshing refining in the region of the wing, the prism grid parameters are employed. The reference signs 1, 2 and 3 in Figure 5 represent the velocity inlet, pressure outlet and symmetric boundary conditions, respectively.

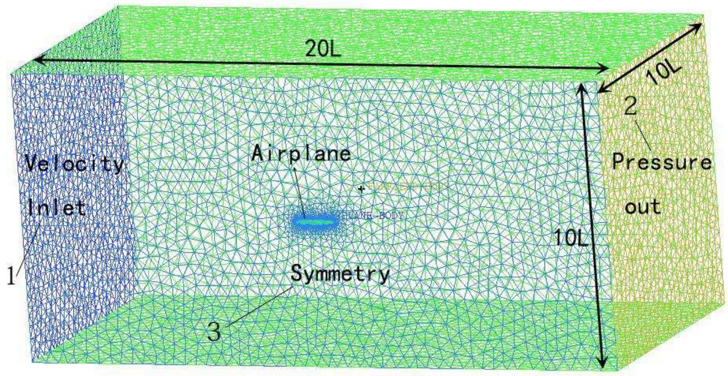

Figure 5. Symmetric computational domain grid and boundary conditions

To verify grid independence, four cases of mesh densities are adopted to compute the lift and drag coefficients. Based on 3-degree of the variable camber of wing in Figure 5(b), the Reynolds number (Re) is calculated as 406508 at angles of attack of 6° and 10°, respectively. The numerical results are summarized in Table 2, which indicate that the differences between cases 2 and 3, and between cases 3 and 4 are less than 2%. To achieve a relatively high resolution of grid, the mesh of case 2 is utilized for the present numerical simulation and the total number of cells and nodes are 36062701 and 4527750, respectively.

This step allows us to obtain more accurate estimations of the flow characteristics as well as to make a preparation for flight test. Four types of whole variable camber wing aircraft models are selected, which are defined as 1-degree wing model, 3-degree wing model, 5-degree wing model and 7-degree wing model, respectively.

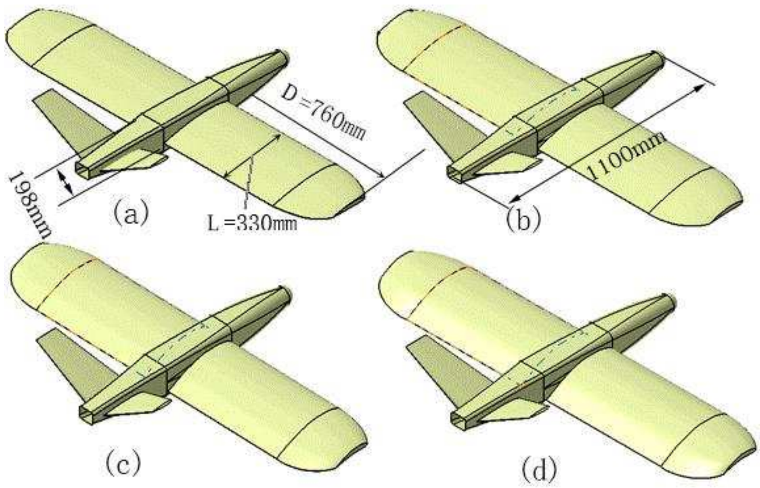

Figure 6. Four models of the variable camber wing aircraft. (a) 1-degree wing model, (b) 3-degree wing model, (c) 5-degree wing model, (d) 7-degree wing model (D: Half of span)

Table 2. Research on grid independence for variable camber aircraft at Re=406508 and angle

of attack of 6 ° and 10 °

Case	Number of cells	Angle of attack 6 °		Angle of attack 10 °	
		C_L	C_d	C_L	C_d
1	15000000	0.682	0.11051	0.826	0.4362
2	36062701	0.629	0.10458	0.778	0.1320
3	58500000	0.635	0.108352	0.786	0.1421
4	85250000	0.621	0.108452	0.782	0.1315

4. Aerodynamic performance of AVCW

The flow characteristics of flow field of changeable camber wing are computed with two-dimensional and three-dimension incompressible continuous equations. According to Navier-Stokes (N-S) equations, a series of numerical simulations are performed under different initial conditions to investigate the aerodynamic performance of the variable camber airfoil and wing, as below.

4.1 2D aerodynamic characteristics

Based on the research purpose, four kinds of design variable camber airfoil and two types of conventional airfoil are selected, as described in Figure 1. The angle of attack varies from 0° to 25°, of which simulation results are shown in Figure 7-9.

Figure 7 shows that the aerodynamic performance greatly affects the lift coefficient owing to the change of the airfoil camber. The lift coefficient gradually increases with the increase of airfoil camber at the same angles of attack, which can be observed in Figure 7. In addition, it can be discovered that the camber is beneficial to enhance the lift performance when the angle of attack is smaller than 15°. With further increase of the angle of attack, the lift coefficient gradually decreases, which may cause flow separation due to the unsteady vortex of the near airfoil surface. Therefore, 15° corresponds to the critical angle of attack in the numerical results. In general, the variable camber airfoil has a stall angle of attack at about 15° and is larger than those of the Clark Y and AH-79-100C airfoil, leading to improved lift aerodynamic characteristics.

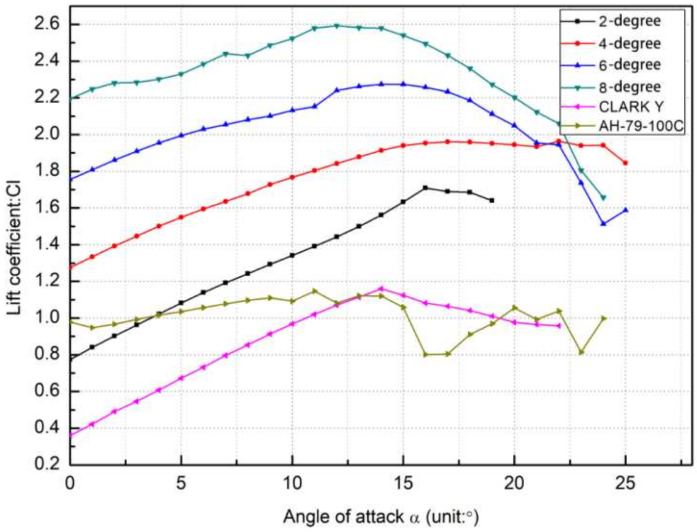

Figure 7. Lift coefficient distribution of 2D different variable airfoils and angle of attack

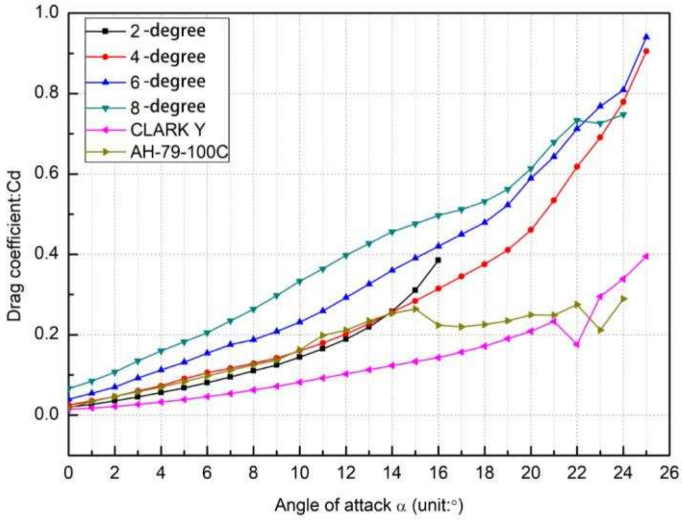

Figure 8. Drag coefficient distribution of 2D different variable airfoils and angle of attack

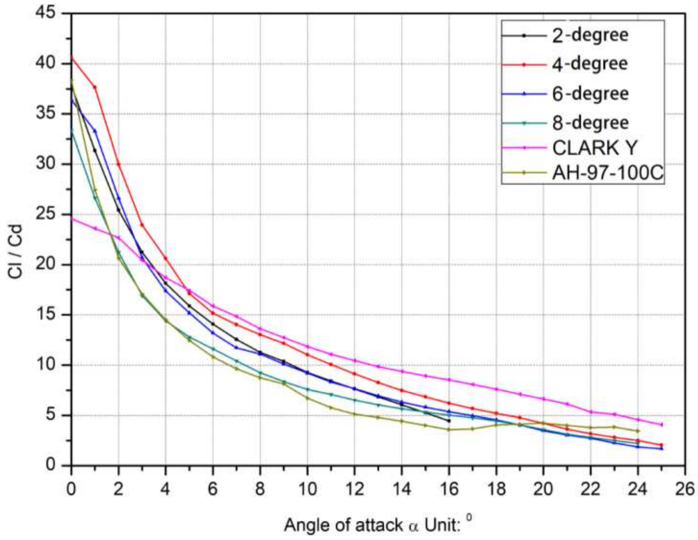

Figure 9. Pole curve of 2D different variable camber airfoils and angle of attack

From Figure 8, it can be seen that the drag coefficient of airfoil also increases with the growth of the angle of attack, which mainly owes to the excessive ??? camber for the design airfoil. It also means that further modify variable camber airfoil is needed in future work. As shown in Figure 9, while the angle of the airfoil camber is smaller than 4-degree, it is in favor of enhancing the ratio of lift to drag. Compared with Clark Y and AH-79-100C airfoil, appropriate airfoil camber design strengthens aerodynamic performance. However, the greater initial camber angle of airfoil deteriorates the aerodynamic performance. It is mainly caused by laminar-turbulence transition around the airfoil, eventually leading to decreased lift coefficient and increased drag coefficient. On condition that the numerical simulation results in this work, 15° angle of attack is recommended to apply for the design variable camber airfoil.

4.2 3D aerodynamic characteristics

In order to validate the aerodynamic performance of varying camber wing in three-dimensional configurations, four types of changeable camber wing are chosen and computed. To enhance the efficiency and accuracy of calculation, the variable camber wing aircraft model is simplified to a half model, but the tail is included. As shown in Figure 10 -11, the camber change of wing has a significant effect on the aerodynamic performance.

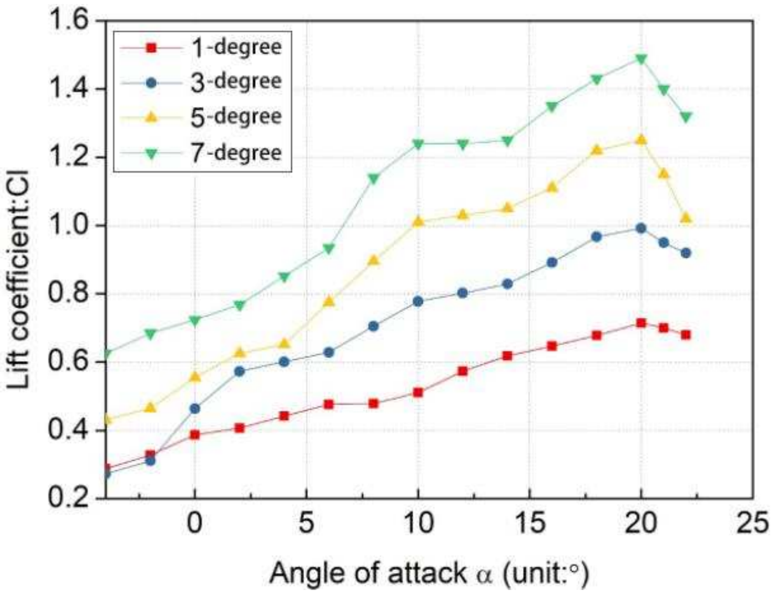

Figure 10. The effect of lift coefficients with different 3D wing camber and angle of attack

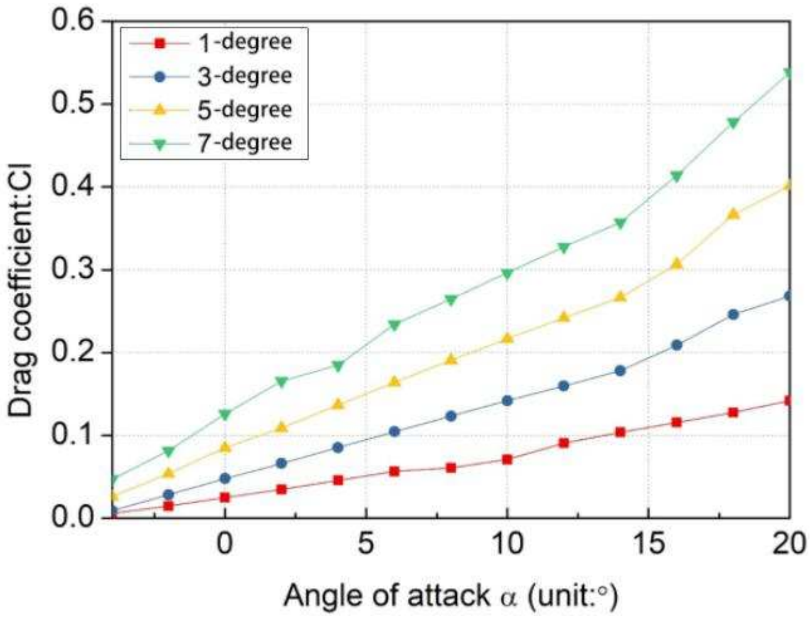

Figure 11. The effect of drag coefficients with different 3D wing camber and angle of attack

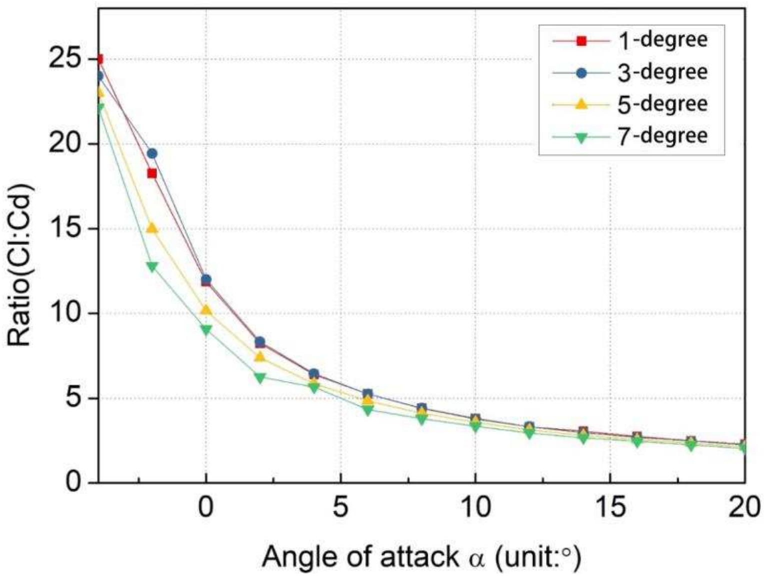

Figure 12. The effect of the pole curve with different 3D wing camber and angle of attack

Figure 10-12 show the lift coefficient, drag coefficient and pole curve distribution of variable camber wing from -2° to 20° of angle of attack, respectively. Compared with 2D numerical results, the trend of the curve distribution is similar. Adjustable camber can effectively control lift coefficient under three-dimensional wing situations. However, it is noteworthy that there are a few distinctions here. First of all, the stall angle of attack of the entire variable camber wing is about 18°, greater than the result from 2D simulation in Figure 7, which is mainly due to the impact of the tail and the overall layout on the flow characteristics of UAV. It also can be seen that the lift coefficient is smaller compared with the airfoil numerical results (Fig. 7) and the drag coefficient is similar (Fig. 8 and Fig. 11) in the range from 0° to 20° angle of attack. Figure 12 shows that when the camber is lower than 3-degree, reducing the camber of the wing can increase the ratio of lift to drag. Taking into consideration the above-mentioned error factors, two-dimensional and three-dimensional models of the calculation results can be used to as a reference for design and flight test of AVCW UAV.

5. AVCW aircraft manufacture and ground test

In order to verify the flight advantage of the complete changeable camber wing, an electric prototype model is manufactured with take-off weight of four kilograms. In the design of the entire varying camber wing aircraft, a widely used Talon UAV (X-UAV fat fixed-wing aircraft) fuselage is adopted for the purpose of easy comparison and reduced error of production. Two experimental prototype models are built, one of which is the combination of the Talon UAV fuselage and the whole variable camber wing (see Figure 13a), and the other is the unmodified Talon UAV fuselage and wing (see Figure 13b). It is remarkable that the above variable camber wing design parameters are identical with Talon UAV wing. The detail parameters are shown in Table 3.

The processes of UAV manufacture and assembly are demonstrated as follows, which are presented in detail in the supporting material.

(1) The changeable camber wing part is designed in AutoCAD software, (2) The wing rib, wing spar, DRS structure, skins and other components are cut by laser, (3) The variable camber wing and the fuselage are assembled, (4) The steering gear, motor, battery, and adaptive flight control system are installed, and (5) The whole AVCW aircraft testing on ground is completed.

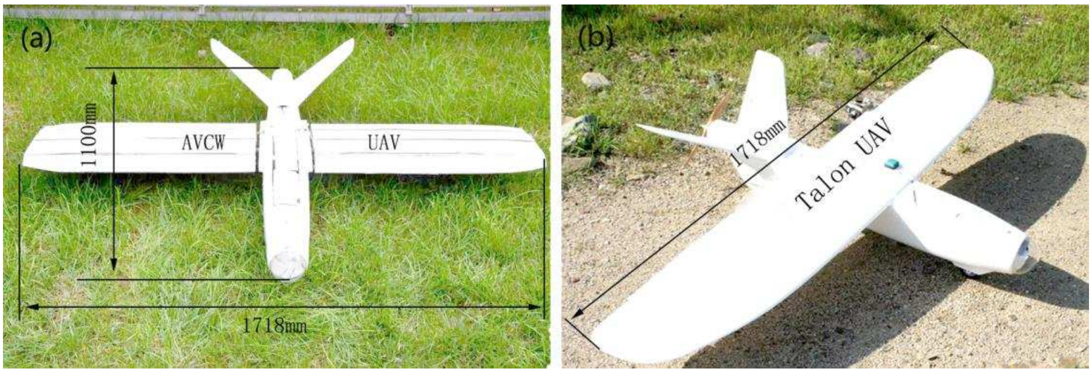

Figure 13. The flight test of whole AVCW aircraft and traditional fixed-wing Talon aircraft, (a) AVCW UAV, and (b) Talon UAV

Table 3 General parameters of the electric prototype model

Item	value
Wing span / mm	1718
Wing area / m^2	0.5
Take-off weight / kg	4
Fuselage length / mm	1100

It is worth noting that the variable camber wing structure is made of light aircraft wood structure, with thickness of 1mm, 2mm, 3mm respectively In addition, the skin arranged in a way liking overlapping fish scales to obtain a smooth aerodynamic shape. In order to reach the flexible flight for changeable camber wing aircraft, the adaptive flight control system is developed based on the PX4 and Mission planner secondary development. In the case of the ACS is not equipped, the expense of the whole variable camber wing prototype model is less than 500 $. The production and fabrication costs of AVCW UAV can be significantly reduced in the future during mass production.

6. Flight-test validation

Noticeably, it is of great significance to verify the validity of numerical simulation results, the effectiveness of the performance indicators in design and reasonability of structural design among flight experiment. Thereby, an X-UAV fat fixed-wing aircraft and a nearly similar constant wing camber aircraft based on the AVCW UAV adjusted by the ACS, are chosen to for the flight trial result. First of all, the equivalent configuration parameters of UAV are adopted. Besides, two identical standard 2000 mAh batteries, battery charger and voltmeter are prepared before the flight test. In the same flying state, including straight line of 20 meters per second and uniform airline, a 10-minutes flight test is carried out. The voltage of the battery is obtained based on the results of five flight experiments for every airplane model. However, it should be noted here that the voltage of the battery before the flight is 16.5V and the battery are fully charged for repeatability experiment. The results indicate that the average voltage drop of 5 flight trials for different aircraft protypes is 0.8V and 0.78V, respectively. The above flight-test results are in good quantitative agreement. In general, the changeable camber wing design is considered to be believable.

To analyze the real-time flight characteristics of AVCW aircraft, two groups comparison flight-test experiments are conducted, in which one group of flight experiment are the AVCW UAV and X-UAV fat fixed-wing aircraft, and the other group of tests are AVCW UAV and constant camber state when the camber of the variable camber wing aircraft is defined as 3-degree, one of which the AVCW aircraft flight test is presented in the Supporting Material.

7.1 Experiment 1

The experimental system is a comparative trial between an X-UAV fat fixed-wing aircraft and an AVCW UAV. Flight tests are attained with the following procedure. Firstly, two 5000 mAh 4S batteries of the same model, battery charger, a voltmeter and transmitter power control (Futaba T4YF-2.4GHz transmitter) are provided. Using a calibrated voltmeter, the voltage of the battery is measured to 16.4V and 16.5V, correspondingly, which is utilized to provide power for the AVCW UAV and X-UAV fat fixed-wing aircraft. Before the experiment is performed, the ACS is debugged, and three types of flight cruise models are set.

Table 4 displays the details of the experiment conditions, including the cruise model is 12m/s, 14m/s and 16m/s and cruise time is 5 minutes. In a similar flight environment, this contains the flight altitude, atmospheric temperature, atmospheric humidity and airflow, etc. Noted that five flight experiments for every aircraft protype model are carried out and the battery is fully charged for repeatability experiment. The flight-test results reveal that the mean voltage drop of the battery is 1.2V in the adaptive flight state. Whereas for a X-UAV fat fixed-wing aircraft under the same flight missions, the voltage drop is 1.7V. Table 4.

Comparison of flight test of adaptive camber aircraft and Talon aircraft

Test	Aircraft type	Number of Tests	Cruise setting	Voltage drop	Dissipative energy
Test 1	AVCW	5	5min, 12m/s 5min, 14m/s 5min, 16m/s	1.2V	21600000J
Test 2	Talon	5	5min, 12m/s 5min, 14m/s 5min, 16m/s	1.7V	30600000J

Based on Test 1 and Test 2, the complete changeable camber wing in flexible flight condition can save electricity about 0.5V relative to the X-UAV fat fixed-wing aircraft. It can be estimated that the whole adaptive variable camber flight improves the flight efficiency by 29.4% compared with X-UAV fat fixed-wing aircraft under the same flight mission. The whole AVCW technology breaks the constraints of energy and power systems for cruise time. The application of this technology may promote the technical revolution in the field of fixed-wing UAV, which is of great significance to the development of the UAV industry and has a high scientific research value.

7.2 Experiment 2

The experimental system setting and results are presented in Table 5. Effects on the flight performance for the comparative experiment of the whole AVCW and 3-degree constant camber wing are investigated. Based on Table 5, two 2000mAh batteries of the uniform capacity are applied. The cruise velocity of Test 1 and Test 2 is about 20 m/s under the same flight states. It should be noted that five flight trials for prototype model are performed and the battery is fully charged for repeatable experiment.

The experimental results are shown as follows: when ACS is adopted, the cruise time of whole AVCW aircraft is longer than that of fixed wing camber at 3-degree. Because the UAV is equipped with an ACS, it can achieve real-time change of for wing camber during the entire flight to accomplish the minimum flight drag. It can be observed that the results show the average cruise time of the whole AVCW wing and 3-degree fixed camber wing are 45 minutes and 35 minutes, respectively. Compared with the Table 5, a conclusion can be drawn: adding the ACS to UAV can increase the flight efficiency by 28.6%.

Table 5. Comparison of flight test of adaptive camber aircraft and 3-degree constant wing

Test	Aircraft type	Number of tests	Power supply	Cruise setting	Cruise time
Test 1	AVCW	5	2000mAh	20m/s	45minutes
Test 2	3-degree constant camber wing	5	2000mAh	20m/s	35minutes

7. Conclusions

In the paper, an innovative double rib sheet structure is proposed to control the position of a whole camber of the wing by a relative rotational motion of the DRS groove contact surface. Numerical simulation is applied to investigate the effect of varying camber airfoil and wing on the aerodynamic performance of UAV. In order to realize further flight experiment study, the whole changeable camber wing prototype model with an ACS is manufactured. Two groups of controlled flight-test experiment are conducted to demonstrate aerodynamic performance benefits of AVCW UAV. The following conclusions can be drawn as

1) An innovative DRS structure is invented, which accomplishes the change of the whole variable camber wing without increasing the overall structural weight of the wing except for the actuating device.

2) The load transfer mode of the new design of variable camber wing structure is groove surface contact, which allows the structure to reach enormous capacity for loads.

4) As compared with Clark Y airfoil and AH-79-100C airfoil, adjustable camber airfoils have shown better aerodynamic performance and stalled characteristics.

5) The flight experiment (experiment 1) results show that comparison with the design scheme of traditional fixed wing of Talon UAV, the whole AVCW technology improves aircraft flight efficiency by 29.4%.

6) Using the experimental setup and programs described in trial 2, the results show that adding the ACS to UAV improves the flight efficiency by 28.6%.

Further study is necessary to explore the appropriate number of wing rib sections and investigate the effects of the relative rotation angle between different sections on aerodynamic performance of the whole AVCW UAV.

Acknowledgement

The work was supported by the Innovation and Entrepreneurship Foundation No. XXXXXX to the Beihang university, and the Beihang Aviation Innovation Practice Base.

Reference

[1] T. Mihetec, Utilization of the Flexible Airspace Structure in the Flight Efficiency Optimisation, Hrvatska znanstvena bibliografija i MZOS-Svibor, DOI (2012).

[2] D. Koch, Quiet, efficient fans for space flight: An overview of NASA's technology development plan, Journal of the Acoustical Society of America, 127 (2010) 1838-1838.

[3] M. Bashir, P. Rajendran, Morphing Wing Technologies, 2017.

[4] W.H. Su, S.S.M. Swei, G.M.G. Zhu, Optimum Wing Shape of Highly Flexible Morphing Aircraft for Improved Flight Performance, J. Aircr., 53 (2016) 1305-1316.

[5] S. POWERS, L. WEBB, E. FRIEND, W. LOKOS, Flight test results from a supercritical mission adaptive wing with smooth variable camber, 28th National Heat Transfer Conference, 1992, pp. 4101.

[6] J.N. Kudva, Overview of the DARPA Smart Wing Project, J.intell.mater.syst.struct, 15 (2004) 261-267.

[7] J.N. Kudva, B.P. Sanders, J.L. Pinkertonflorance, E. Garcia, Overview of the DARPA/AFRL/NASA Smart Wing Phase II program, Proc Spie, 4332 (2001) 383-389.

[8] B.K. Stanford, Static and Dynamic Aeroelastic Tailoring with Variable-Camber Control, Journal of Guidance Control and Dynamics, 39 (2016) 2522-2534.

[9] Y. Tian, T. Wang, P. Liu, P. Feng, Aerodynamic/mechanism optimization of a variable camber Fowler flap for general aviation aircraft, Sci. China-Technol. Sci., 60 (2017) 1144-1159.

[10] H.D. Li, H.S. Ang, Preliminary airfoil design of an innovative adaptive variable camber compliant wing, J. Vibroeng., 18 (2016) 1861-1873.

[11] W. Yin, Stiffness requirement of flexible skin for variable trailing-edge camber wing, Sci. China-Technol. Sci., 53 (2010) 1077-1081.

[12] T. Yokozeki, A. Sugiura, Y. Hirano, Development of Variable Camber Morphing Airfoil Using Corrugated Structure, J. Aircr., 51 (2014) 1023-1029.

[13] F. Gandhi, P. Anusonti-Inthra, Skin design studies for variable camber morphing airfoils, Smart Materials & Structures, 17 (2008).

[14] H. Zhu, W.D. Liu, C.S. Zhao, Morphing Aircraft and Its Morph-driving Techniques, Machine Building & Automation, DOI (2010).

[15] S. Kota, R. Osborn, G. Ervin, D. Maric, P. Flick, D. Paul, Mission Adaptive Compliant Wing – Design , Fabrication and Flight Test Mission Adaptive Compliant Wing, DOI (2006).

[16] L. Jun, Q. Yanhua, B. Tao, Y. Zhehui, L. Yan, Development of a morphing wing with adaptive capability, Acta Aerodynamica Sinica, 27 (2009) 505-508.

[17] S. Barbarino, R. Pecora, L. Lecce, A. Concilio, S. Ameduri, L. De Rosa, Airfoil Structural Morphing Based on SMA Actuator Series: Numerical and Experimental Studies, Journal of Intelligent Material Systems and Structures, 22 (2011) 987-1004.

[18] W. Liu, H. Zhu, S. Zhou, Y. Bai, Y. Wang, C. Zhao, In-plane corrugated cosine honeycomb for 1D morphing skin and its application on variable camber wing, Chinese Journal of Aeronautics, 26 (2013) 935-942.

[19] W. Yin, L. Liu, Y. Chen, J. Leng, Variable camber wing based on pneumatic artificial muscles, in: J. Leng, A.K. Asundi, W. Ecke (Eds.) Second International Conference on Smart Materials and Nanotechnology in Engineering2009.

[20] W. Yin, L. Liu, Y. Chen, Y. Liu, J. Leng, Pneumatic artificial muscle and its application on driving variable trailing-edge camber wing, in: M.B. McMickell, K.M. Farinholt (Eds.)

Industrial and Commercial Applications of Smart Structures Technologies 20102010.
[21] I. ANSYS, ANSYS FLUENT User's Guide DOI (2011).
[22] A. Fluent, ANSYS FLUENT 14.5 Theory Guide, DOI (2012).